ARTICLE
https://doi.org/10.23919/XXX.2020.000000
iEnergy

Resilience of Gas Interchangeability in Hydrogen-Blended Integrated Electricity and Gas Systems: A Transient Approach With Dynamic Gas Composition Tracking

Sheng Wang[1], Hongxun Hui[1] and Pierluigi Siano[2]

ABSTRACT

Green hydrogen can be produced by consuming surplus renewable generations. It can be injected into the natural gas networks, accelerating the decarbonization of energy systems. However, with the fluctuation of renewable energies, the gas composition in the gas network may change dramatically as the hydrogen injection fluctuates. The gas interchangeability may be adversely affected. To investigate the ability to defend the fluctuated hydrogen injection, this paper proposes a gas interchangeability resilience evaluation method for hydrogen-blended integrated electricity and gas systems (H-IEGS). First, gas interchangeability resilience is defined by proposing several novel metrics. Then, A two-stage gas interchangeability management scheme is proposed to accommodate the hydrogen injections. The steady-state optimal electricity and hydrogen-gas energy flow technique is performed first to obtain the desired operating state of the H-IEGS. Then, the dynamic gas composition tracking is implemented to calculate the real-time traveling of hydrogen contents in the gas network, and evaluate the time-varying gas interchangeability metrics. Moreover, to improve the computation efficiency, a self-adaptive linearization technique is proposed and embedded in the solution process of discretized partial derivative equations. Finally, an IEEE 24 bus RTS and Belgium natural gas system are used to validate the proposed method.

KEYWORDS

Integrated electricity and gas systems, gas composition, hydrogen, resilience, renewable energy

Green hydrogen is one of the most appealing solutions to the decarbonization of energy systems. It is usually produced by power-to-gas (PTG) by consuming surplus renewable generations [1,2]. The green hydrogen can be then injected into the pipelines, and transported to other locations for further use. Recently, many small trials have been implemented in China, the UK, the US, etc., which demonstrate the feasibility of blending hydrogen into natural gas pipelines [3–5]. For example, the hydrogen blending demonstration project in Zhangjiakou, China, 2020, is estimated to provide more than 4 million m^3 hydrogen to residential users and vehicles per year, which can reduce approximately 3000 t carbon emissions [6].

However, excessive injections of hydrogen can affect the gas compositions, and consequently jeopardize gas interchangeability. Interchangeability is used to describe whether two gases are interchangeable. If the new gas mixtures can be used to substitute the original natural gas without affecting the operation of gas appliances, then the interchangeability of the new gas mixture can be considered qualified [7]. Due to the lower heat value of hydrogen, if too much hydrogen is blended, the new gas mixture cannot produce the same amount of heat energy compared with the original gas. Then, the performance of gas appliances, such as gas water heaters, can be affected. This issue is more severe in the case of green hydrogen. Because renewable generation is stochastic, the gas interchangeability of gas will become more unpredictable. Therefore, it is essential to closely monitor and regulate gas interchangeability in the presence of green hydrogen.

Since gas interchangeability is dominated by gas composition, some researchers are dedicated to the gas composition tracking problem. For example, the steady-state gas composition simulation model with the injection of alternative gas is studied in [8]. The gas composition tracking problem is combined with the electricity system operation in [9] to reach a global optimum. The impacts of hydrogen produced by distributed photovoltaic generation on the gas system are investigated in [10]. The probabilistic gas flow with multiple gas types is established in [11] considering uncertainties. Though the gas composition can be simulated or optimized in these studies, the impacts of hydrogen on gas interchangeability are not quantified. As a result, we still do not know if the gas composition is qualified in terms of interchangeability,

1 State Key Laboratory of Internet of Things for Smart City, University of Macau, Taipa, Macao SAR, China;
2 Department of Management & Innovation Systems, University of Salerno, Salerno, Italy.
Address correspondence to Hongxun Hui, hongxunhui@um.edu.mo

or keep the gas composition in an interchangeable range. Recently, some works start to pay attention to maintaining gas interchangeability. For example, the security of the gas mixtures is considered in the optimal operation of hydrogen-blended integrated electricity and gas system (H-IEGS) with alternative gas in [12]. It has also been integrated into the robust operation of H-IEGS with hydrogen and renewable energies in [13].

Nevertheless, the previous studies usually adopt static gas security criteria, such as the Wobbe index, combustion potential, etc., straightforwardly to calculate gas interchangeability. Though these static criteria can measure the values of gas interchangeability quantitatively under a specific given condition at a certain time point, they cannot fully reflect the dynamic abilities of the H-IEGS to maintain gas interchangeability during time-varying operating conditions. In another word, these studies cannot fully utilize the flexibility of the gas system itself to defend the gas interchangeability violations. For example, when the hydrogen injection is increased, the hydrogen fraction can increase suddenly near the injection point, and the gas interchangeability near that point may be inferior. However, the gas system may increase the gas flow rate near that injection point gradually, pushing the gas interchangeability back to the acceptable range. This ability of the gas system to defend the gas interchangeability variations, and to recover gas interchangeability to the normal level, can be defined as the resilience of gas interchangeability.

Though the resilience of the electricity system [14, 15] or gas system [16, 17] regarding the energy supply capability is widely studied, the resilience of the H-IEGS with respect to the gas interchangeability against the fluctuating renewable generations has not been investigated yet. The evaluation of gas interchangeability resilience requires near real-time captures of the dynamics of gas flow, and more importantly, gas composition variations due to the fluctuation of hydrogen injections. These two kinds of dynamics are governed by partial derivative equations (PDE), which are very challenging to incorporate in the optimal operation of H-IEGS efficiently. Especially for the gas composition dynamics, though recently a few studies start to incorporate them into the coordinate operation of H-IEGS [18], the solution efficiency still needs improvement. Moreover, its impact on gas interchangeability has not been investigated either.

To address the research gaps, this paper proposes a novel resilience evaluation method for gas interchangeability in the H-IEGS. Other contributions are summarized as follows:

(1) Novel metrics are defined from multiple dimensions to evaluate the resilience of gas interchangeability. Compared with traditional static gas security metrics, the proposed metrics can: a) better reflect the capability of the gas system to defend gas interchangeability violations caused by the hydrogen injections; b) calculate the accumulated gas interchangeability loss, which is more in line with the real gas safety regulations [19].

(2) A two-stage gas interchangeability management scheme is proposed. It entails solving the steady-state optimal electricity and hydrogen-gas energy flow (SOEF) problem first to determine the desired operating state of the H-IEGS. In the second stage, the dynamic gas composition tracking (DGCT) problem is solved to determine the optimal path of reaching the desired operating state, as well as using the gas flow dynamics to mitigate the gas interchangeability loss during this process.

3) A self-adaptive linearization technique is used to solve the discretized PDEs. The reference points of the gas flow, and gas property coefficient (i.e., specific gravity, compressibility factors, etc) are updated based on a gap criterion, so that the computation efficiency can be improved while the accuracy can still be guaranteed.

1 Gas interchangeability resilience

1.1 Gas interchangeability

The traditional method, such as the Dutton method, which is widely used in the UK, Australia, etc., usually adopts three metrics, i.e., Wobbe index (WI), Incomplete Combustion Factor (ICF), and Soot Index (SI) to measure the gas interchangeability [20]. However, these regulations are established without considering the participation of hydrogen. Since hydrogen has a higher flame speed, here we use another metric, the Weaver flame speed factor (FS), to further guarantee gas interchangeability [21]. Thus, we have:

$$(1-\sigma)WI_i^{min} \le WI_{i,k} \le (1+\sigma)WI_i^{max} \tag{1}$$

$$ICF_{i,k} \le (1+\sigma)ICF_i^{max} \tag{2}$$

$$SI_{i,k} \le (1+\sigma)SI_i^{max}; \tag{3}$$

$$(1-\sigma)FS_i^{min} \le FS_{i,k} \le (1+\sigma)FS_i^{max}; \tag{4}$$

$$0 \le \chi_{i,k}^{hy} \le (1+\sigma)\chi_i^{hy,max} \tag{5}$$

$$WI_{i,k} = GCV_{i,k} / \left((S^{ng})^{\frac{1}{2}} + (S^{ng})^{-\frac{1}{2}} S_{i,k}\right) \tag{6}$$

$$ICF_{i,k} = \left(WI_{i,k} - 50.73 + 0.03\chi_{i,k}^{ng}(\chi_{i,k}^{pr} + \chi_{i,k}^{ni})\right)/1.56 - 0.01\chi_{i,k}^{hy} \tag{7}$$

$$SI_{i,k} = 0.896 tan^{-1}(0.0255\chi_{i,k}^{ng}\chi_{i,k}^{pr} - 0.0233\chi_{i,k}^{ng}\chi_{i,k}^{ni} - 0.0091\chi_{i,k}^{hy} + 0.617) \tag{8}$$

$$FS_{i,k} = (\chi_{i,k}^{ng} fs^{ng} + \chi_{i,k}^{hy} fs^{hy})/(AF + 5\chi_{i,k}^{ng}\chi_{i,k}^{ni} - 18.8\chi_{i,k}^{ng}\chi_{i,k}^{ox} + 1) \tag{9}$$

$$GCV_{i,k} = \chi_{i,k}^{ng} GCV^{ng} + \chi_{i,k}^{hy} GCV^{hy} \tag{10}$$

$$S_{i,k} = \chi_{i,k}^{ng} S^{ng} + \chi_{i,k}^{hy} S^{hy} \tag{11}$$

where (1) - (5) are the constraints for WI, ICF, SI, and the molar fraction of hydrogen, respectively; $WI_{i,k}$, $ICF_{i,k}$, $SI_{i,k}$, and $FS_{i,k}$ are the WI, ICF, SI, and FS of the gas mixture at gas bus i in time step k, respectively; WI_i^{min} and WI_i^{max} are the lower and upper bounds of WI, respectively; ICF_i^{max} and SI_i^{max} are the upper bounds of ICF and SI, respectively; FS_i^{min} and FS_i^{max} are the lower and upper bounds of FS, respectively; σ is the relaxation factor of the interchangeability constraints, which can be used for to guarantee the feasibility; $\chi_{i,k}^{hy}$

and $\chi_{i,k}^{ng}$ are the molar fractions of hydrogen and natural gas in the gas mixture at gas bus i in step k, respectively; $\chi_i^{hy,max}$ is the upper bound of molar fraction of hydrogen; (6) - (9) are the calculation methods for WI, ICF, SI, and FS, respectively; $GCV_{i,k}$ and $S_{i,k}$ are the gross caloric value (GCV) and specific gravity at gas bus i in time step k, respectively; S^{ng} and S^{hy} are the specific gravity of natural gas and hydrogen, respectively; fs^{ng} and fs^{hy} are the flame speed factors of natural gas and hydrogen, respectively; $\chi_{i,k}^{pr}$, $\chi_{i,k}^{ni}$, and $\chi_{i,k}^{ox}$ are the molar fractions of propane, nitrogen, and oxygen in the natural gas, respectively; AF is the air-fuel ratio; (10) and (11) are the calculation methods of GCV and specific gravity, respectively.

1.2 Resilience of gas interchangeability

Resilience can be defined as the ability to defend, endure, and recover from the impacts of a triggering event [22]. In the presence of uncertain and fluctuating hydrogen injections, the resilience of gas interchangeability can be defined as the ability of the H-IEGS to maintain the gas interchangeability within the acceptable range. Or, in cases where the violation of gas interchangeability constraints is inevitable, it also refers to the ability to quickly recover to acceptable interchangeability.

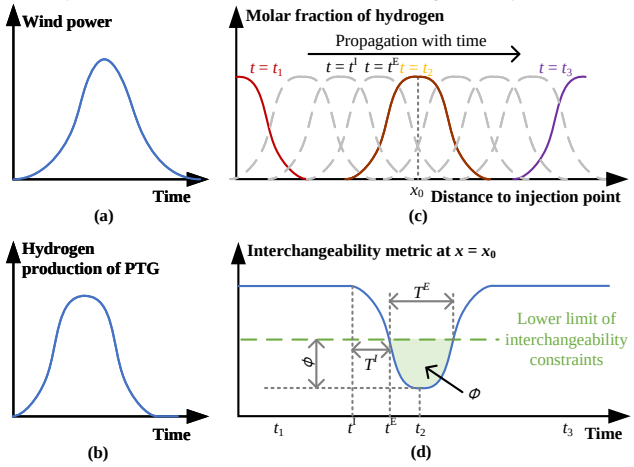

Fig. 1 Resilience of gas interchangeability. (a) Wind generation, (b) hydrogen production of PTG, (c) traveling of the molar fraction of hydrogen, (d) resilience metrics.

To define the metrics that measure the resilience of gas interchangeability, an illustrative example is shown in Fig. 1. Suppose there is a spike in wind generation, as shown in Fig. 1(a). Then, the hydrogen production of PTG also increases correspondingly. Fig. 1(c) shows the travel of the hydrogen content in the gas network. At different times (e.g., t_1, t_2, and t_3), the distribution of the molar fraction in the pipeline is different. As the peak of the hydrogen molar fraction curve gradually moves from the injection point to distant locations, the gas interchangeability metrics at a specific location, e.g, $x = x_0$, is shown in Fig. 1(d). Several key features are marked to characterize the resilience of gas interchangeability from multiple dimensions. ϕ is the maximum gas interchangeability loss during this period. For example, if the y-axis represents the WI, then:

$$\phi_i = |\min\{WI_{i,k} - WI_i^{min}\}|, k \in \mathcal{K} \tag{12}$$

where $\mathcal{K}$ is the set of all time steps.

$T^I = t^E - t^I$ is the settling time. T^I can reflect the ability of the gas system to maintain gas interchangeability; T^E is the length of the enduring phase. It can reflect the ability of the gas system to recover from the interchangeability violation. Φ is the total interchangeability loss accumulated over time, which can be calculated by:

$$\Phi_i = \sum_{k \in \mathcal{K}} \phi_{i,k} \tag{13}$$

2 Two-stage gas interchangeability management scheme

During the operation, due to the fluctuation of the hydrogen injection, gas interchangeability may be affected. The H-IEGS will take active measures to defend against gas interchangeability loss. For example, if the hydrogen injection is high, the system operator may choose to increase the gas flow near the hydrogen injection point to dilute the hydrogen fraction, although it is not the most economic way to do so in normal states.

Considering that renewable generation is difficult to predict, here we propose a two-stage gas interchangeability management scheme, as shown in Fig. 2. In the first stage, the SOEF is solved first to determine the desired operating state of H-IEGS with minimum gas interchangeability loss. However, due to the slower gas flow and gas composition dynamics, the system may not able to reach the desired state immediately. Therefore, in the second stage, the DGCT problem is performed to optimize the path toward the desired state (i.e., the real-time operating condition of the H-IEGS with less gas interchangeability loss and more hydrogen injection).

2.1 First stage: steady-state optimal electricity and hydrogen-gas flow problem

In this stage, the SOEF is performed for each renewable generation capacity level to determine the desired operating condition of the H-IEGS, as illustrated in Fig. 2. The objective is to minimize the total cost, including electricity generation and gas purchasing costs, as shown in (14) (the notation of k is omitted for conciseness).

$$\min \sum_{i \in \mathcal{I}} \sum_{l \in \mathcal{L}_i^{tpp}} f_{i,l}^{cst}(g_{i,l}^{tpp}) + \sum_{i \in \mathcal{I}} \sum_{l \in \mathcal{L}_i^{gs}} \rho_{i,l}^{s} q_{i,l}^{gs} \tag{14}$$

where $\mathcal{I}$ is the set of buses; $\mathcal{L}_i^{tpp}$ and $\mathcal{L}_i^{gs}$ are sets of traditional fossil power plants and gas sources at bus i, respectively; $f_{i,l}^{cst}(\cdot)$ is the cost function of traditional fossil power plant l at bus i; $g_{i,l}^{tpp}$ and $q_{i,l}^{gs}$ are the electricity generation and gas production of traditional fossil power plant l and gas source l at bus i, respectively; $\rho_{i,l}^{s}$ is the gas production price of the gas source l at bus i.

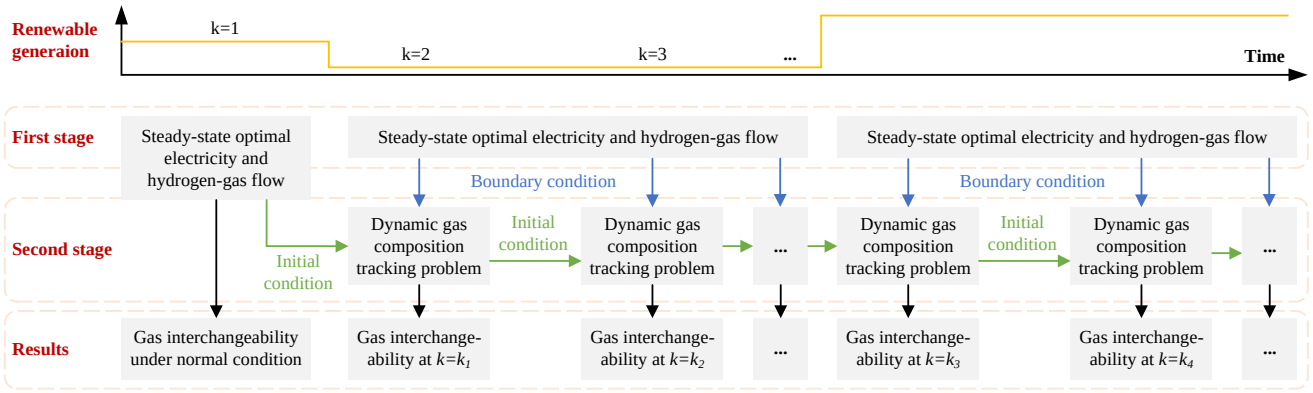

Fig. 2 Framework of two-stage gas interchangeability management scheme.

The optimization model is subject to:

1) Gas system constraints:

$$GCV^{ng} q_i^{d,ng,0} = q_i^{d,ng} GCV^{ng} + q_i^{d,hy} GCV^{hy} \tag{15}$$

$$[q_i^{d,ng}, q_i^{d,hy}] = [\chi_{i,k}^{ng}, \chi_{i,k}^{hy}](q_i^{d,ng} + q_i^{d,hy}) \tag{16}$$

$$(q_{ij}^{ng} + q_{ij}^{hy})^2 = \pi^2 D_{ij}^5 (F_{ij} r_{ij} L_{ij} z_{ij} T^{ng})^{-1} \gamma_{ij} (p_i^2 - p_j^2) \tag{17}$$

$$\sum_{l \in \mathcal{L}_i^s} q_{i,l}^s - q_i^{d,ng} - \sum_{l \in \mathcal{L}_i^{gpp}} q_{i,l}^{gpp,ng} - \sum_{j \in \mathcal{J}_i} q_{ij}^{ng} = 0 \tag{18}$$

$$\sum_{l \in \mathcal{L}_i^{ptg}} q_{i,l}^{ptg} - q_i^{d,hy} - \sum_{l \in \mathcal{L}_i^{gpp}} q_{i,l}^{gpp,hy} - \sum_{j \in \mathcal{J}_i} q_{ij}^{hy} = 0 \tag{19}$$

$$q_i^{in,ng} = \sum_{j \in \mathcal{J}_i} (\gamma_{ij} - 1) q_{ij}^{ng}/2 + \sum_{l \in \mathcal{L}_i^{gs}} q_{i,l}^s \tag{20}$$

$$q_i^{in,hy} = \sum_{j \in \mathcal{J}_i} (\gamma_{ij} - 1) q_{ij}^{hy}/2 + \sum_{l \in \mathcal{L}_i^{ptg}} q_{i,l}^{ptg} \tag{21}$$

$$[\chi_i^{ng}, \chi_i^{hy}] = [q_i^{in,ng}, q_i^{in,ng}]/(q_i^{in,ng} + q_i^{in,ng}) \tag{22}$$

$$R_i = \chi_i^{ng} R^{ng} + \chi_i^{hy} R^{hy} \tag{23}$$

$$r_{ij} = \left((1+\gamma_{ij}) R_i + (1-\gamma_{ij}) R_j\right)/2 \tag{24}$$

$$\chi_{ij} = \left((1+\gamma_{ij}) \chi_i + (1-\gamma_{ij}) \chi_j\right)/2 \tag{25}$$

$$q_i^{d,ng}, q_i^{d,hy} \geq 0 \tag{26}$$

$$q_{i,l}^{gs,min} \leq q_{i,l}^{gs} \leq q_{i,l}^{gs,max} \tag{27}$$

$$(\gamma_{ij} - 1) q_{ij}^{max}/2 \leq q_{ij} \leq (\gamma_{ij} + 1) q_{ij}^{max}/2 \tag{28}$$

$$p_i^{min} \leq p_i \leq p_i^{max}, i \neq i^{ref} \tag{29}$$

$$p_{i^{ref}} = p^{ref} \tag{30}$$

$$\chi_{i,k}^{ng} + \chi_{i,k}^{hy} = 1, 0 \leq [\chi_{i,k}^{ng}, \chi_{i,k}^{hy}] \leq 1 \tag{31}$$

where (15) indicates that the total heat energy of the gas demands of natural gas and hydrogen should equal the total heat energy of the original gas demand measured in natural gas; $q_i^{d,ng,0}$ is the gas demand at bus i measured in original natural gas; $q_i^{d,ng}$ and $q_i^{d,hy}$ are the gas demand of natural gas and hydrogen at bus i, respectively; (16) indicates that the gas composition of the gas consumption of gas demand should equal the gas composition at the exact gas bus; (17) is the Weymouth equation for gas mixtures; q_{ij}^{ng} and q_{ij}^{hy} are the gas flow rates of natural gas and hydrogen in the pipeline that connects bus i and bus j (it also refers to pipeline ij), respectively; p_i and p_j are the nodal gas pressure of buses i and j, respectively; D_{ij}, L_{ij}, and F_{ij} are the diameter, length, and friction factor of the pipeline ij, respectively; r_{ij} and z_{ij} is the gas constant and compressibility factor of the gas mixture in pipeline ij, respectively; T^{ng} is the temperature of gas; $\gamma_{ij} \in \{-1, 1\}$ is the gas flow direction, where $\gamma_{ij} = 1$ indicates that the gas flows from bus i to j, and $\gamma_{ij} = -1$ indicates otherwise; (18) and (19) are the nodal gas flow balances of natural gas and hydrogen, respectively; J_i is the set of gas buses connected to bus i; $\mathcal{L}_i^{ptg}$ and $\mathcal{L}_i^{gpp}$ are the sets of PTGs and gas-fired power plants at gas bus i, respectively; $q_{i,l}^{ptg}$ is the hydrogen production of PTG l at bus i; $q_{i,l}^{gpp,ng}$ and $q_{i,l}^{gpp,hy}$ are the natural gas and hydrogen consumptions of gas-fired power plant l at bus i, respectively; (20) and (21) are the calculation formulations of nodal injections of natural gas and hydrogen at bus i, respectively; $q_i^{in,ng}$ and $q_i^{in,hy}$ are the nodal injections of natural gas and hydrogen at bus i, respectively; (22) is the gas mixing equation; (23) and (24) are the calculation methods for the gas constants of the gas mixtures at bus i and in the pipeline ij, respectively; R^{ng} and R^{hy} are the gas constants of natural gas and hydrogen, respectively; (25) is the calculation method for the gas composition in pipelines; χ_{ij} is the gas composition in the pipeline ij; (26)-(31) are the bounds for optimization variables; $q_{i,l}^{gs,min}$ and $q_{i,l}^{gs,max}$ are the lower and upper bounds of the gas production of gas source l at bus i, respectively; q_{ij}^{max} is the capacity of pipeline ij; p_i^{min} and p_i^{max} are the lower and upper bounds of the gas pressure at bus i, respectively; i^{ref} is the reference gas bus, which should be equal to p^{ref} during the operation.

2) Electricity system constraints:

$$\sum_{l \in \mathcal{L}_i^{tpp}} g_{i,l}^{tpp} + \sum_{l \in \mathcal{L}_i^{gpp}} g_{i,l}^{gpp} + g_i^{wf} - \sum_{l \in \mathcal{L}_i^{ptg}} g_{i,l}^{ptg} - g_i^d - \sum_{j \in \mathcal{J}_i} g_{ij} = 0 \tag{32}$$

$$g_{ij} = (\theta_i - \theta_j)/X_{ij} \tag{33}$$

$$g_{i,l}^{gpp} = \eta_{i,l}^{gpp} (q_{i,l}^{gpp,ng} GCV^{ng} + q_{i,l}^{gpp,hy} GCV^{hy}) \tag{34}$$

$$g_{i,l}^{ptg} \eta_{i,l}^{ptg} = q_{i,l}^{hy} GCV^{hy} \tag{35}$$

$$|g_{ij}| \leq g_{ij}^{max} \tag{36}$$
$$g_{i,l}^{tpp,min} \leq g_{i,l}^{tpp} \leq g_{i,l}^{tpp,max} \tag{37}$$
$$g_{i,l}^{gpp,min} \leq g_{i,l}^{gpp} \leq g_{i,l}^{gpp,max} \tag{38}$$
$$g_{i}^{wf,min} \leq g_{i}^{wf} \leq g_{i}^{wf,max} \tag{39}$$
$$q_{i,l}^{gpp,ng}, q_{i,l}^{gpp,hy} \geq 0 \tag{40}$$
$$q_{i,l}^{hy} \geq 0 \tag{41}$$

where (32) is the nodal balance of electricity flow; $g_{i,l}^{tpp}$ and $g_{i,l}^{gpp}$ are the electricity generations of traditional fossil power plant and gas-fired power plant l at bus i, respectively; g_i^{wf} is the electricity of the wind farm at bus i; $g_{i,l}^{ptg}$ is the electricity consumption of PTG l at bus i; g_i^d is the electricity demand at bus i; (33) is the DC electricity power flow equation; g_{ij} is the electricity flow on the electricity branch ij; θ_i is phase angle of the voltage at bus i; X_{ij} is the reactance of branch ij; (34) and (35) are the models of gas-fired power plant and PTG, respectively; $\eta_{i,l}^{gpp}$ and $\eta_{i,l}^{ptg}$ are the efficiencies of gas-fired power plant and PTG l at bus i, respectively; (36)-(41) are the bounds for optimization variables; g_{ij}^{max} is the capacity of the electricity branch ij; $g_{i,l}^{tpp,min}$ and $g_{i,l}^{tpp,max}$ are the lower and upper bounds of the electricity generation for traditional fossil power plant l at bus i, respectively; $g_{i,l}^{gpp,min}$ and $g_{i,l}^{gpp,max}$ are the lower and upper bounds of the electricity generation for gas-fired power plant l at bus i, respectively; $g_i^{wf,min}$ and $g_i^{wf,max}$ are the lower and upper bounds of the electricity generation for wind farm at bus i, respectively.

2.2 Second stage: dynamic gas composition tracking

The first stage defines the desired operating state of H-IEGS. Then, in the second stage, the DGCT is implemented to optimize the path in which the H-IEGS reaches the desired operating state. Therefore, the optimization problem is formulated on each time step, with the objective of minimizing the deviations to the desired operating state, as well as the gas interchangeability loss:

$$\min \sum_{i\in\mathcal{I}} \sum_{l\in\mathcal{L}_i^{ptg}} ||q_{i,l,k}^{ptg} - q_{i,l,k}^{ptg*}|| + \mu\sigma \tag{42}$$

where $q_{i,l,k}^{ptg*}$ is the solution of the gas production of the PTG in the SOEF problem; μ is the penalty factor.

It is subject to:

1) Gas dynamic constraints:

The dynamics of gas flow, as well as the traveling of specific gas content, are governed by three PDEs, namely, continuity equation, motion equation, and advective equation. Their discrete form in an isothermal and horizontal pipeline can be written as [18]:

$$A_{ij}\Delta x(\rho_{ij,m-1,k} - \rho_{ij,m-1,k-1} + \rho_{ij,m,k} - \rho_{ij,m,k-1}) + 2\Delta t\rho_0(q_{ij,m,k} - q_{ij,m-1,k}) = 0 \tag{43}$$

$$2\Delta x^{-1}(\rho_{ij,m-1,k} + \rho_{ij,m,k})(p_{ij,m,k} - p_{ij,m-1,k}) + (\rho_{ij,m-1,k} + \rho_{ij,m,k})\rho^{stp}(A_{ij}\Delta t)^{-1}(q_{ij,m,k} - q_{ij,m,k-1} + q_{ij,m-1,k} - q_{ij,m-1,k-1}) + \gamma_{ij}\Theta^2(q_{ij,m-1,k} + q_{ij,m,k})^2 = 0 \tag{44}$$

$$A_{ij}\Delta x(\rho_{ij,m-1,k} + \rho_{ij,m,k})(\chi_{ij,m-1,k}^{hy} - \chi_{ij,m-1,k-1}^{hy} + \chi_{ij,m,k}^{hy} - \chi_{ij,m,k-1}^{hy}) + 2\Delta t\rho_0(q_{ij,m-1,k} + q_{ij,m,k})(\chi_{ij,m,k-1}^{hy} - \chi_{ij,m-1,k-1}^{hy}) = 0, \quad ij \in \mathcal{P}, m = 2,3,...,M, k = 2,3,...,K \tag{45}$$

where m is the index for pipeline segments; M and K are the numbers of pipeline segments and time steps, respectively; Δt and Δx are the time step and length step, respectively; A_{ij} is the cross-sectional area of pipeline ij; $\Theta = (2\pi D_{ij}^5 F_{ij})^{-\frac{1}{2}}$; ρ^{stp} is the density of natural gas at standard temperature and pressure condition. It is worth noting that the discretization forms of the variables should be chosen carefully in order to keep a good balance between accuracy, feasibility, and stability. Normally, the central difference scheme has better accuracy, but is more likely to cause oscillation issues. Therefore, the implicit differentiation scheme is applied as well.

2) Initial and boundary conditions:

The above PDEs are formulated for each pipeline in the gas system. To derive the operating state of a dynamic system, initial and boundary conditions are required. The initial condition is determined by the SOEF (for k=1) or the operating state at the last time step (for k>1), which is obtained by solving the DGCT problem at the last time step, as shown in Fig.2:

$$p_{ij,m,1} = p_{ij,m}^*, k = 1 \tag{46}$$
$$p_{ij,m,k} = p_{ij,m,k-1}^{**}, k > 1 \tag{47}$$

where $p_{ij,m}^*$ is the solution of the pressure in the first stage OEF problem; $p_{ij,m,k-1}^{**}$ is the solution of the DGCT problem at the last time step. The initial conditions of gas density, gas composition, and gas flow, can be given similarly.

The boundary condition is given by the pipelines it is connected with. For example, the gas pressures at the connecting point should be equal. The gas composition at the beginning of the pipeline should be equal to the upstream gas bus. Therefore, we have:

$$p_{ij,1,k} = p_{i,k} = p_{ij',1,k}, \forall j' \in \mathcal{J}_i \tag{48}$$
$$p_{ij,M,k} = p_{j,k} = p_{i'j,M,k}, \forall i' \in \mathcal{I}_j \tag{49}$$
$$(\gamma_{ij} + 1)\chi_{ij,1,k,n}^{hy} = (\gamma_{ij} + 1)\chi_{i,k,n}^{hy} \tag{50}$$
$$(\gamma_{ij} - 1)\chi_{ij,M,k}^{hy} = (\gamma_{ij} - 1)\chi_{j,k}^{hy} \tag{51}$$

where $\mathcal{I}_j$ is the set of buses that are connected with bus j. The boundary condition for the gas flow is given by the nodal gas flow balance equation, similar to (18) and (19).

3) Gas state equation:

$$p_{ij,m,k} = z_{ij,m,k} r_{ij,m,k} T^{ng} \rho_{ij,m,k} \tag{52}$$

4) Other constraints: The DGCT problem should also follow constraints (1)-(11), (15), (16), and (18)-(41).

It is worth noting that because the DGCT problem is formulated on each time step, the state variables at the last time step (e.g., $p_{ij,m,k-1}$, $1_{ij,m,k-1}$, etc.) are given. After solving the DGCT problem, the state variables at the next time step can be obtained.

3 Solution method

The optimization problems in the first and second stages are both nonlinear and nonconvex. To solve the problem more tractably, an adaptive linearization method is proposed. The idea of the adaptive linearization method is to approximate the nonlinear terms using Taylor expansion or other kinds of linearization methods, and the reference point of the Taylor expansion will be updated if the state of the system changes dramatically. With this idea, the optimization problem can become more tractable without increasing the computation burden, and the accuracy can also be improved compared with fixed reference points.

3.1 Adaptive linearizations of two-stage gas interchangeability management problem

In the first stage SOEF problem, the nonlinearities exist in the: 1) the nodal consumption of gas demand (16); 2) the Weymouth equation (17); 3) the nodal gas mixing equation (22). They are reformulated to:

$$\begin{aligned} q_i^{d,hy} = \hat{\chi}_{i,k}^{hy}(\hat{q}_i^{d,ng} + \hat{q}_i^{d,hy}) + \chi_{i,k}^{hy}(\hat{q}_i^{d,ng} + \hat{q}_i^{d,hy}) \\ +\hat{\chi}_{i,k}^{hy}(q_i^{d,ng} + q_i^{d,hy}) \\ (q_i^{ng} + q_i^{hy})(\hat{q}_{ij}^{ng} + \hat{q}_{ij}^{hy}) \end{aligned} \tag{53}$$

$$= \pi^2 D_{ij}^5 (F_{ij} r_{ij}^* L_{ij} z_{ij}^* T^{ng})^{-1} \gamma_{ij} (P_i - P_j) \tag{54}$$

$$\begin{aligned} q_i^{in,hy} = \hat{\chi}_{i,k}^{hy}(\hat{q}_i^{in,ng} + \hat{q}_i^{in,hy}) + \chi_{i,k}^{hy}(\hat{q}_i^{in,ng} + \hat{q}_i^{in,hy}) \\ +\hat{\chi}_{i,k}^{hy}(q_i^{in,ng} + q_i^{in,hy}) \end{aligned} \tag{55}$$

where $\hat{\chi}_{i,k}^{hy}$, $\hat{q}_i^{d,ng}$, $\hat{q}_i^{d,hy}$, $\hat{q}_{ij}^{ng}$, $\hat{q}_{ij}^{hy}$, $\hat{q}_i^{in,ng}$, and $\hat{q}_i^{in,hy}$ are the reference points of $\chi_{i,k}^{hy}$, $q_i^{d,ng}$, $q_i^{d,hy}$, q_{ij}^{ng}, q_{ij}^{hy}, $q_i^{in,ng}$, and $q_i^{in,hy}$, respectively; $P_i = p_i^2$ is the square of gas pressure.

In the second stage problem, the nonlinearities exist in the: 1) motion equation (44); 2) advective transport equation (45); 3) gas state equation (52). They are reformulated as [23]:

$$\begin{aligned} 2(\Delta x)^{-1}(\hat{\rho}_{ij,m-1} + \hat{\rho}_{ij,m})\Big((p_{ij,m,k} - p_{ij,m-1,k}) \\ -(p_{ij,m,k-1} - p_{ij,m-1,k-1})\Big) + (\hat{\rho}_{ij,m-1} + \hat{\rho}_{ij,m}) \\ \rho^{stp}(A_{ij}\Delta t)^{-1}(q_{ij,m,k} - q_{ij,m,k-1} + q_{ij,m-1,k} \\ -q_{ij,m-1,k-1}) + \gamma_{ij}\Theta^2(\hat{q}_{ij,m-1} + \hat{q}_{ij,m}) \\ \Big((q_{ij,m-1,k} + q_{ij,m,k}) - (q_{ij,m-1,k-1} + q_{ij,m,k-1})\Big) = 0 \end{aligned} \tag{56}$$

$$\begin{aligned} A_{ij}\Delta x(\hat{\rho}_{ij,m-1} + \hat{\rho}_{ij,m})(\chi_{ij,m-1,k} - \chi_{ij,m-1,k-1} \\ +\chi_{ij,m,k} - \chi_{ij,m,k-1}) + 2\Delta t\rho_0(\hat{q}_{ij,m-1} + \hat{q}_{ij,m}) \\ (\chi_{ij,m,k-1} - \chi_{ij,m-1,k-1}) = 0 \end{aligned} \tag{57}$$

where $\hat{\rho}_{ij,m}$ and $\hat{q}_{ij,m}$ is the reference points for $\rho_{ij,m}$ and $q_{ij,m}$, respectively.

The reference point is initially selected according to the solution in the first stage SOEF problem (e.g., $\hat{\rho}_{ij,m} = \rho_{ij,m}^*$) when $k = 1$. When $k > 1$, the following criterion is set to determine whether the reference point should be updated:

$$|\boldsymbol{x}_k^{**} - \boldsymbol{x}_{k-1}^{**}| / |\boldsymbol{x}_k^{**} + \boldsymbol{x}_{k-1}^{**}| > \epsilon \tag{58}$$

where ϵ is the threshold for the criterion; $\boldsymbol{x}_k^{**}$ represents the set of the solutions for all state variables (e.g., gas pressure, gas flow, etc.) in the DGCT problem at time step k. If (58) is satisfied, then update the reference point of $\boldsymbol{x}$ as $\hat{\boldsymbol{x}} = \boldsymbol{x}_k^{**}$.

3.2 Solution procedure

The whole solution procedure is elaborated as follows:

Step 1: Initialize the system data, including the wind speed, system structure, energy demands, physical data of components, etc. Set the total time steps K, and the time and space resolution for PDE problems Δx and Δt.

Step 2: Solve the SOEF problem by replacing the gas production of PTG with natural gas according to [12]. Set the solutions as the reference points (e.g., $q_{i,j}^*$) for $k = 1$.

Step 3: For each wind level, solve the first stage SOEF problem based on (1)-(11), (14)-(15), (18)-(21), (23)-(41), and (53)-(55).

Step 4: For $k = 1$, set the solution of the first stage SOEF problem as the reference point and the initial condition for the second stage DGCT problem according to (46)-(47).

Step 5: For each time step k, solve the DGCT problem according to (1)-(11), (15), (16), (18)-(43), (46)-(52), (56), and (57).

Step 6: Set the solution in Step 5 as the initial condition for the DGCT problem at $k + 1$. See if the criterion (58) is satisfied. If yes, update the reference point. Repeat Step 5 for $k + 1$ until all the time steps have been iterated.

Setp 7: Evaluate the gas interchangeability resilience metrics according to Section 1.2.

4 Case studies

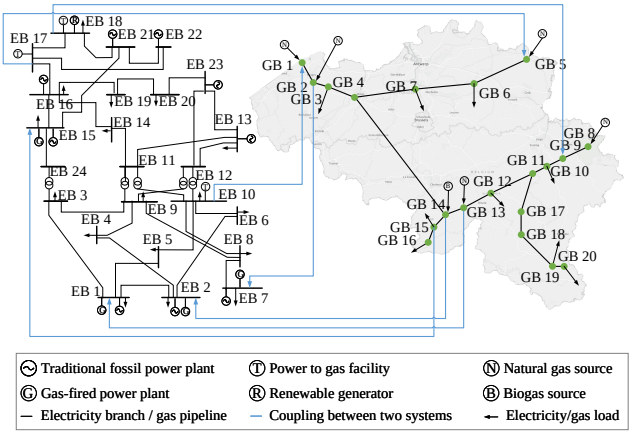

Fig. 3 H-IEGS test case composed by IEEE 24 bus RTS and Belgium natural gas system.

In this section, the IEEE 24 bus RTS and Belgium gas system are used to validate the proposed method. The topological structure of the two coupling systems is presented in Fig. 3. The detailed data of the two systems can be found in [24] and [25], respectively. Three PTGs are installed at electricity bus #10, 17, 18, respectively, which are also connected with gas bus # 1, 5, 9, respectively. The capacities of the PTGs are 2 Mm^3/day. The wind farm is located at electricity bus #18, with a generation capacity of 800 MW. The time and space resolutions are set to 1800 s and 1000 m, respectively.

4.1 Validation of proposed method

First, we validate the proposed method in terms of both computation efficiency and credibility. We assume only the PTG at electricity bus #18 is available. The wind generation is assumed to increase from 100 MW to 800 MW at $k = 2$. As a result, the hydrogen production of the PTG increases from 1.55 Mm^3/day to 2 Mm^3/day.

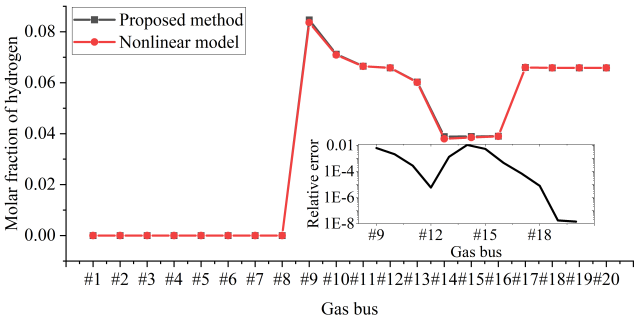

Fig. 4 Comparison of the solutions with different methods.

We compare our method with a general nonlinear solver (IPOPT). The total computation time of our method with $K = 48$ is 1.53 s, which is 98.94 % faster than the IPOPT solver (143.69 s). The solutions of the nodal molar fraction of hydrogen right after the hydrogen injection, at which time the system state changes dramatically and is most likely to cause large errors, are compared in Fig. 4. As we can see, the relative error between the proposed method and the IPOPT is tiny. The errors at all buses do not exceed 1%. The largest errors occur at gas bus #9 (the injection point) and #14 (where the pure natural gas and hydrogen-natural gas mixtures are mixed). At other gas buses, the errors are almost neglectable.

4.2 Gas interchangeability resilience of different gas buses

In this subsection, we investigate the gas interchangeability resilience of different buses. We assume only the PTG at electricity bus #18 is available. The wind generation is assumed to increase from 100 MW to 800 MW at $k = 2$.

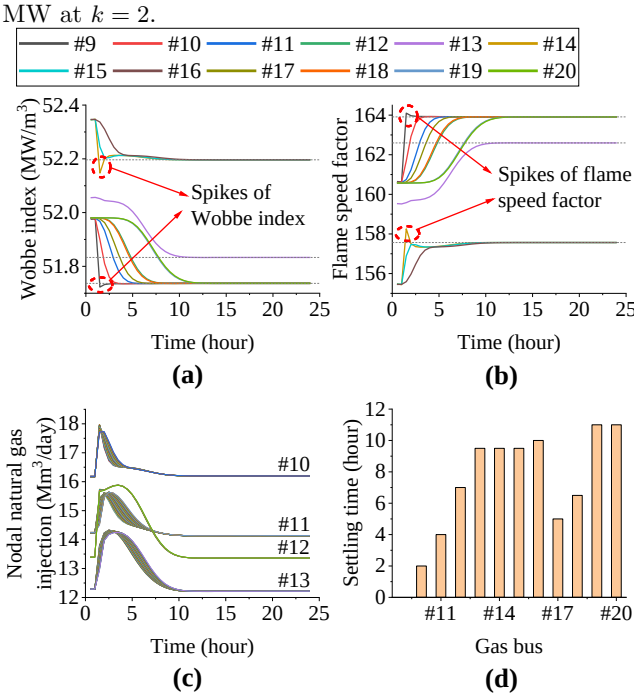

Fig. 5 Operating conditions with hydrogen injection at gas bus #9. (a) Wobbe index, (b) flame speed factor, (c) nodal injections of natural gas, (d) nodal settling time.

First, some critical gas interchangeability metrics (e.g., the Wobbe index and flame speed factor) when the hydrogen is injected into gas bus #9, are presented as an example in Fig. 5. We can find that, with the injection of hydrogen, due to its lower GCV and higher flame speed, the Wobbe index and flame speed factor gradually decrease and increase with time, respectively. However, the spikes of gas interchangeability could be generated in some gas buses (gas bus #9 and 14 in this case) near the hydrogen injection time point, as shown in Fig. 5. (a) and (b). This is because the suddenly injected hydrogen can be stacked near the injection points. These spikes are not caused by numeral simulations, and cannot be neglected because they will cause unexpected temporal violations of gas interchangeability metrics. For example, the maximum and accumulated Wobbe index losses at gas bus #9 and #14 are 0.014 MW/m^3, 0.049 MW/m^3, 49.07 MJ/m^3, and 88.20 MJ/m^3, respectively.

To defend against the gas interchangeability loss, the gas system raises the gas flow rate of natural gas near the injection point to dilute the molar fraction of hydrogen. For example, as shown in Fig. 5. (c), the nodal natural gas injections at gas buses #10, 11, 12, and 13 increase dramatically near the injection time point. Fig. 5. (d) shows the settling times of gas buses in response to the hydrogen injection. It can be seen that the settling time is longer with the longer distance between the gas bus and the injection point. For example, gas buses #16 and 20 are at the ends of two pipeline routes, and their settling times can reach up to 10 and 11 hours. It shows that the transient process of gas composition cannot be neglected in the gas interchangeability evaluation. The longer settling time means those gas buses can have more time to prepare and respond to the hydrogen injection, which increases the resilience of these buses against the hydrogen injection.

Table 1 Gas interchangeability resilience with different hydrogen injection points

Scenario	S1	S2	S3	S4
Injection point	#1	#5	#8	#9
Gas production of PTG when k >2 (Mm^3/day)	2.00	1.16	2.00	2.00
Total settling time (h)	38.5	4	93	85
Maximum Wobbe index loss (MW/m^3)	0.027	0	0.048	0.063
Accumulated Wobbe index loss (MJ/m^3)	47.80	0	86.94	137.3
Maximum flame speed factor loss	0.373	0	0.676	0.749
Accumulated flame speed factor loss	671.9	0	1217	1913

Following this idea, we can study the resilience of the gas system with the hydrogen injected into other different gas buses, i.e., gas buses #1, 5, and 8. The gas interchangeability metrics are shown in Table. 1. We can observe that different gas buses have different resilience against hydrogen injection. Comparing S3 and S4, we can find that the upper stream locations are more suitable for hydrogen injections. Compared with S4, the total settling time is longer in S3, which means the gas system will have more time to respond to mitigate the gas interchangeability loss. The maximum Wobbe index and flame speed factor losses in S3 are 23.81% and 9.75% lower than that in S4, which means the gas interchangeability losses are also lower. The accumulated Wobbe index and flame speed losses in S8 are also 36.68% and 36.38% lower than in S4, which means the gas interchangeability loss will recover faster in S3.

Gas buses #1, 5, and 8 are all at the beginning of pipeline routes. Observing these scenarios, we can find that the gas interchangeability shows various patterns when the hydrogen is blended in different gas buses. Comparing S2 with S1 and S3, we find that although the gas interchangeability loss is lower, the gas production of PTG is also significantly lower. This is because the gas flow rate near gas bus #5 is relatively low, which cannot support the large volume hydrogen injection without causing gas interchangeability loss. Comparing S1 and S3, we find that the settling time of S1 is shorter than S3. This is because when hydrogen is injected in gas bus #1, it only propagates to limited gas buses (i.e., #2-4, 6-7, and 14-16). These gas buses are relatively closer to gas bus #1, and thus the gas system will have less time window to regulate gas interchangeability. In contrast, other gas interchangeability resilience metrics in S1, such as maximum and accumulated Wobbe index and flame speed factor loss, are lower than in S3. This means the gas system will have a stronger ability to adapt if the hydrogen is injected into the gas bus #1.

4.3 Gas interchangeability resilience during daily operation

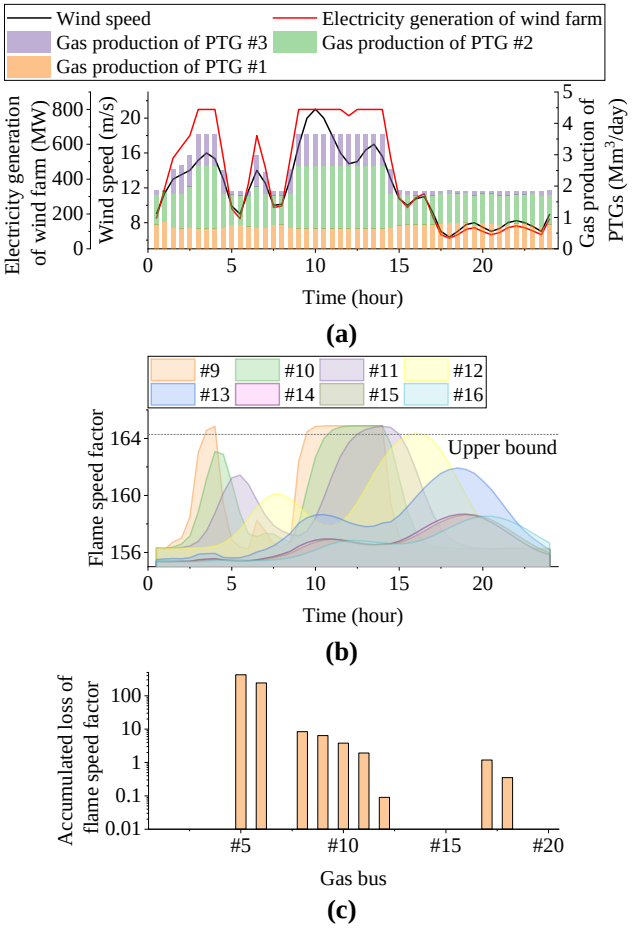

Fig. 6 Daily operating conditions. (a) Wind speed, electricity generation of the wind farm, and gas production of PTGs, (b) nodal flame speed factors, (c) accumulated loss of flame speed factors.

In this case, the proposed gas interchangeability resilience evaluation method is further applied to daily operations. The wind speed data is obtained from National Oceanic and Atmospheric Administration [26]. All the PTGs are committed in this case. The operating conditions of the H-IEGS are presented in Fig. 6.

From Fig. 6.(a), we find that the hydrogen production of PTGs follows the wind speed generally. The highest wind speed appears around 3:00-4:00 and 9:00-14:00, during which the hydrogen production also

reaches its maximum values. PTG #2 is less affected by the wind, which contributes to hydrogen production significantly over the operational horizon. Since PTG #2 is connected with gas bus #8, we further present the flame speed factors along the critical pipeline route which starts from gas bus #8 to #16, as shown in Fig.6. (b). The distribution pattern of the flame speed factor along that route verifies the theory that we developed in the last subsection. The gas buses that are closer to the hydrogen injection point are more likely to violate the upper bound of the gas interchangeability metrics (e.g., gas bus #9). For the downstream gas buses, such as #12-16, they will have more time windows to increase the gas flow rate of the natural gas to dilute the molar fraction of hydrogen, and thus the gas interchangeability is more resilient. Observing from the whole H-IEGS, not only the gas buses near #8, but also the gas buses near #5, are likely to violate the gas interchangeability constraints, as shown in Fig. 6. (c). This is because #5 also has hydrogen injections. Unlike gas bus #8 where the gas flow rate is large, the gas source in the gas bus #5 is relatively small. Therefore, the gas system will have less flexibility to dilute the molar fraction of hydrogen in gas bus #5, and the gas interchangeability resilience is also inferior.

5 Conclusions

This paper proposes a gas interchangeability resilience evaluation method in integrated electricity and gas systems with the injection of hydrogen. Novel gas interchangeability resilience metrics are proposed. A two-stage gas interchangeability resilience management scheme is proposed to improve the interchangeability considering the traveling of hydrogen content across the gas network. A self-adaptive linearization technique is proposed to improve the computation efficiency while maintaining a satisfying accuracy.

The numerical results show that our solution method can improve the computation efficiency by 98.94%, while the relative error is controlled with 1%. We also find that the upper stream gas bus with a relatively large gas flow rate is more suitable for hydrogen injections in terms of improving the gas interchangeability resilience. For example, the gas interchangeability losses in gas bus #8 under hydrogen injection are lower than in gas bus #1. We also demonstrate the effectiveness of our method in a multi-period daily operation of H-IEGS. With the urging requirement for a low-carbon energy system, the gas interchangeability resilience evaluation method proposed in this paper can help the energy system operators to optimize the operating strategy of the H-IEGS in the future.

Acknowledgements

This work was supported in part by the Science and Technology Development Fund, Macau SAR (File no. SKL-IOTSC(UM)-2021-2023, File no. 0003/2020/AKP) and the Natural Science Foundation of Jiangsu Province, China (Operational reliability evaluation of multi-source and heterogeneous urban multi-energy systems, BK20220261).

Declaration of competing interest

The authors have no competing interests to declare that are relevant to the content of this article.

References

[1] Danny Pudjianto and Goran Strbac. Whole system value of long-duration electricity storage in systems with high penetration of renewables. *iEnergy*, 1(1):114–123, 2022.

[2] Chongqing Kang. Towards net-zero emission power system: Deploy long-duration electricity storage technology for power systems with high penetration of renewables. *iEnergy*, 1(1):11–11, 2022.

[3] Safe operation for one year with 10% hydrogen blending, new breakthrough on first natural gas with hydrogen blending demonstration in China. [Online]. Available: https://new.qq.com/rain/a/20211019A04KVF00.

[4] HyDeploy Project – Project Close Down Report. [Online]. Available: https://hydeploy.co.uk/app/uploads/2022/06/Hy Deploy-Close-Down-Report_Final.pdf.

[5] Report on the first demonstration project of natural gas mixed with green hydrogen for power generation in the United States: 35% hydrogen addition reduces carbon emissions by 14% . [Online]. Available: https://news.bjx.com.cn/html/20220927/1257566.shtml.

[6] Launch of Hebei's first demonstration project on natural gas with hydrogen blending. [Online]. Available: https://news.bjx.com.cn/html/20200917/1105156.shtml.

[7] Harmen de Vries, Anatoli V Mokhov, and Howard B Levinsky. The impact of natural gas/hydrogen mixtures on the performance of end-use equipment: Interchangeability analysis for domestic appliances. *Applied energy*, 208:1007–1019, 2017.

[8] Muditha Abeysekera, Jianzhong Wu, Nick Jenkins, and M Rees. Steady state analysis of gas networks with distributed injection of alternative gas. *Applied Energy*, 164:991–1002, 2016.

[9] Isam Saedi, Sleiman Mhanna, and Pierluigi Mancarella. Integrated electricity and gas system modelling with hydrogen injections and gas composition tracking. *Applied Energy*, 303:117598, 2021.

[10] Marco Cavana, Andrea Mazza, Gianfranco Chicco, and Pierluigi Leone. Electrical and gas networks coupling through hydrogen blending under increasing distributed photovoltaic generation. *Applied Energy*, 290:116764, 2021.

[11] Shenxi Zhang, Shuping Wang, Zhenyuan Zhang, Jiawei Lyu, Haozhong Cheng, Mingyu Huang, and Qingping Zhang. Probabilistic multi-energy flow calculation of electricity–gas integrated energy systems with hydrogen injection. *IEEE Transactions on Industry Applications*, 58(2):2740–2750, 2021.

[12] Sheng Wang, Junyi Zhai, and Hongxun Hui. Optimal energy flow in integrated electricity and gas systems with injection of alternative gas. *IEEE Transactions on Sustainable Energy*, 2023.

[13] Pengfei Zhao, Chenghong Gu, Zechun Hu, Da Xie, Ignacio Hernando-Gil, and Yichen Shen. Distributionally robust hydrogen optimization with ensured security and multi-energy couplings. *IEEE Transactions on Power Systems*, 36(1):504–513, 2020.

[14] Yonghua Song, Can Wan, Xuejun Hu, Hongpei Qin, and Kengweng Lao. Resilient power grid for smart city. *iEnergy*, 1(3):325–340, 2022.

[15] Ektor-Ioannis E Stasinos, Dimitris N Trakas, and Nikos D Hatziargyriou. Microgrids for power system resilience enhancement. *iEnergy*, 1(2):158–169, 2022.

[16] Hongxun Hui, Yulin Chen, Shaohua Yang, Hongcai Zhang, and Tao Jiang. Coordination control of distributed generators and load resources for frequency restoration in isolated urban microgrids. *Applied Energy*, 327:120116, 2022.

[17] Chuan He, Chenxi Dai, Lei Wu, and Tianqi Liu. Robust network hardening strategy for enhancing resilience of integrated electricity and natural gas distribution systems against natural disasters. *IEEE Transactions on Power Systems*, 33(5):5787–5798, 2018.

[18] Sleiman Mhanna, Isam Saedi, Pierluigi Mancarella, and Zihang Zhang. Coordinated operation of electricity and gas-hydrogen systems with transient gas flow and hydrogen concentration tracking. *Electric Power Systems Research*, 211:108499, 2022.

[19] Gas Safety (Management) Regulations. [Online]. Available: https://www.legislation.gov.uk/uksi/1996/551/introduction/made.

[20] Keeman Lee, Jong-Min Kim, Byeonghun Yu, Chang-Eon Lee, and Seungro Lee. Effect of various gas compositions on gas interchangeability and combustion characteristics for domestic appliances. *Journal of Mechanical Science and Technology*, 27:1191–1201, 2013.

[21] Christoper S Weaver. Natural gas vehicles—a review of the state of the art. *SAE transactions*, 98:1190–1210, 1989.

[22] Maedeh Mahzarnia, Mohsen Parsa Moghaddam, Payam Teimourzadeh Baboli, and Pierluigi Siano. A review of the measures to enhance power systems resilience. *IEEE Systems Journal*, 14(3):4059–4070, 2020.

[23] Yongzhi Zhou, Chenghong Gu, Hao Wu, and Yonghua Song. An equivalent model of gas networks for dynamic analysis of gas-electricity systems. *IEEE Transactions on Power Systems*, 32(6):4255–4264, 2017.

[24] Cliff Grigg, Peter Wong, Paul Albrecht, Ron Allan, Murty Bhavaraju, Roy Billinton, Quan Chen, Clement Fong, Suheil Haddad, Sastry Kuruganty, et al. The IEEE reliability test system-1996. A report prepared by the reliability test system task force of the application of probability methods subcommittee. *IEEE Transactions on Power Systems*, 14(3):1010–1020, Aug. 1999.

[25] Daniel De Wolf and Yves Smeers. The gas transmission problem solved by an extension of the simplex algorithm. *Management Science*, 46(11):1454–1465, Nov. 2000.

[26] National oceanic and atmospheric administration. [Online]. Available: https://www.noaa.gov/.